DOI: https://doi.org/10.15407/rpra30.01.041
UDC 621.396.674+520.272.2

**P.L. Tokarsky**

Institute of Radio Astronomy of the NAS of Ukraine
4, Mystetstv St., Kharkiv, 61002, Ukraine
E-mail: p.tokarsky@rian.kharkov.ua

# ELECTRICAL AND NOISE PROPERTIES OF A SYMMETRICAL ANTENNA WITH AN ACTIVE BALUN

***Subject and Purpose.*** *The paper considers an active receiving antenna composed of a symmetrical passive antenna and an active balun that consists of a differential pair of identical low-noise amplifiers and a three-winding differential-input single-ended transformer. The purpose of the paper is developing a model of such an active antenna in the form of an equivalent two-port network with analytically determined electrical and noise parameters.*

***Methods and Methodology.*** *The study is based on methods of antenna theory and noise theory of multi-port networks. The passive antenna is conditionally divided into two identical arms, each regarded as a separate independent antenna, which allows representing the entire active antenna as a three-port network. Then, making allowance for the antisymmetric excitation of the three-port network inputs, it has been converted into a cascade of two two-port networks. The first one corresponds to the passive antenna, and the second to the active balun consisting of one low-noise amplifier with transformers added at input and output .*

***Results.*** *Proceeding from a block diagram of the active antenna, seen as a two-port network, analytical expressions were derived to allow calculations of its scattering matrix and the correlation matrix of noise waves. These permit evaluating electrical and noise parameters of the symmetrical antenna with an active balun. A numerical example is presented, which allows comparing parameters of two symmetrical active antennas, one of which uses the active balun, while the other a low-noise amplifier with a passive balun.*

***Conclusions.*** *The block diagrams developed and the explicit relationships obtained allow a greatly simplified analysis of the symmetric antennas that employ active baluns as they do not need resorting to any specialized software. The results may prove useful for calculating the parameters of low-frequency radio telescopes that employ similar antennas in the capacity of phased array elements.*

***Keywords:*** *symmetrical antenna, active balun, two-port network, scattering matrix, noise waves' correlation matrix.*

## Introduction

The low-frequency radio telescopes, similarly as the communication systems operating in the HF range, often employ symmetrically excited antennas, in particular symmetrical dipoles of various designs. The feeders of such antennas use baluns to transfer the received signal from the symmetrical output of the antenna toward an asymmetrical coaxial cable which transmits the signal to a beam former and further on to the receiver. The LF radio telescopes developed over the past century made use of pas-

Citation: Tokarsky, P.L., 2025. Electrical and noise properties of a symmetrical antenna with an active balun. *Radio Phys. Radio Astron.*, **30**(1), pp. 41—50. https://doi.org/10.15407/rpra30.01.041

© Publisher PH "Akademperiodyka" of the NAS of Ukraine, 2025

This is an Open Access article under the CC BY-NC-ND 4.0 license (https://creativecommons.org/licenses/by-nc-nd/4.0/legalcode.en)

sive baluns. In particular, such baluns, implemented as transmission line-based transformers [1], were used in the Ukrainian radio telescope UTR-2 [2], as well as in the Mexican radio telescope MEXART [3]. Along with those, coaxial baluns [4] were also used in the 22-MHz narrow-band dipole array at Penticton, British Columbia [5], and in the Gauribidanur radio telescope [6] operating at 34.5 MHz.

Due to the development of microelectronics and digital technologies it became possible, at the beginning of the 21st century, to develop LF radio telescopes of a new-generation. They were characterized by the use of active baluns which comprised the central part of their front-end electronics and largely determined the fluctuation sensitivity of the radio telescopes. The Active BalUn (ABU) is a differential input, single-ended output device comprised of a pair of identical low-noise amplifiers (LNA) loaded with a combiner in the form of a three-winding transformer or a magic-T hybrid. The main advantage of the ABU is its ability to suppress intermodulation distortions arising in the single LNA, notably to almost completely suppress second-order distortions and noticeably reduce the level of third-order ones [7, 8].

The hybrid-based ABU is used now in the Long Wavelength Array (LWA) [9]. At the same time, a vast majority of other modern low-frequency radio telescopes, including the Low-Frequency Array (LOFAR) [10], the Eight-meter-wavelength Transient Array [11], the Brazilian low-frequency interferometer [12], Square Kilometer Array (SKA) Log-periodic Antenna [13], Australian SKA pathfinder ASKAP [14], the Murchison Widefield Array [15], the NenuFAR Radio Telescope of Nançay [16], and the Giant Ukrainian Radio Telescope (GURT) [17] (as well as its extension [18]) all employ transformer-based ABUs.

The operation of antenna ABUs, mainly under experimental conditions, has been described in papers like [19—23]. An exception from the trend is paper [23], where a pair of receiving antennas operating either in the common, differential, or a mixed mode is investigated in great detail, both theoretically and experimentally. Part of the results obtained in [23] define the hybrid-based ABU parameters rather extensively. At the same time, theoretical studies of transformer-based ABUs are absent in the literature. The present work is aimed at filling this gap by developing a model of the transformer-based ABU in the form of an equivalent two-port network and analytically determining its electrical and noise parameters in terms of scatter matrices.

## 1. Problem formulation

Consider an active receive antenna (Fig. 1, *a*) consisting of a symmetrical passive antenna and a transformer-based ABU which is composed of two identical LNAs and a symmetrical three-winding transformer T $(L_1 / L_3 = L_2 / L_3 = n^2)$ functioning as a combiner.

We will assume electrical and noise parameters of the LNA to be known and presented here in the form of a scatter matrix **S**, plus its associated noise-wave correlation matrix **C** [24],

$$\mathbf{S} = \begin{pmatrix} S_{11} & S_{12} \\ S_{21} & S_{22} \end{pmatrix}, \quad \mathbf{C} = \begin{pmatrix} C_{11} & C_{12} \\ C_{21} & C_{22} \end{pmatrix}.$$

We will also consider the passive antenna parameters, such as the impedance $Z = R + jX$; radiation efficiency $\eta_r$; effective length $l_e$, and the normalized vectorial radiation pattern (RP) $\vec{F}(\theta,\varphi)$ as known.

Hence, it is necessary to represent the active antenna of Fig. 1, *a* in the form of a cascade of two two-port networks, A and ABU (Fig. 1, *b*), of which the first one corresponds to a symmetrical passive antenna, and the second one to the ABU. Their parameters are to be determined from the **S**-matrices defining the relations between the incident, $a_{in}$ and $a_{out}$, and the reflected $b_{in}$, $b_{out}$ wave amplitudes at the input and output, respectively, of the two-port network, and the **C**-matrix which describes the interaction of the noise waves $c_{in}$ and $c_{out}$ at the output.

## 2. The symmetrical active antenna (SAA) represented as a three-port network

Let us represent the symmetrical, passive receiving antenna of Fig. 1, *a* as an equivalent two-port network A (see Fig. l, *b*). Its output terminals coincide with the actual terminals of the real antenna, while input terminals are connected to a virtual spatial waveguide that transfers into the antenna the energy of the electromagnetic waves propagating through free space. This two-port network can be characterized by a scattering matrix as follows [25],

$$\mathbf{S}^{\mathrm{A}} = \frac{1}{z+1}\begin{pmatrix} z+1-2r\eta_r & 2\sqrt{r\eta_r} \\ 2\sqrt{r\eta_r} & z-1 \end{pmatrix}, \qquad (1)$$

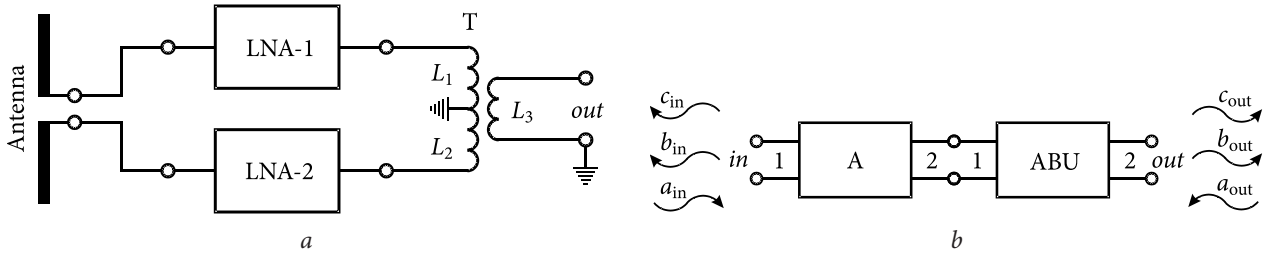


***Fig. 1.*** Block-diagrams of a symmetrical antenna with an ABU: expanded view (*a*); cascaded two-port networks (*b*)

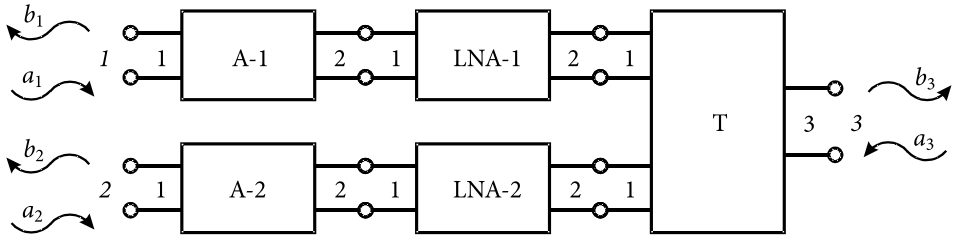


***Fig. 2.*** The SAA as three-port network

where $z = Z / Z_c = r + jx$ is the normalized antenna impedance, and $Z_c$ the system's characteristic impedance.

A uniform, plane EM wave $\dot{\vec{E}}^i$ incident upon the antenna excites an incident wave in the virtual waveguide whose amplitude at the input terminals A is

$$a_{in} = -j\frac{1}{2\sqrt{2}}\frac{l_e}{\sqrt{R\eta_r}}\dot{\vec{E}}^i \cdot \vec{F}(\theta,\varphi). \qquad (2)$$

It is known that parameters of a symmetrical antenna would not change if a virtual perfectly conducting screen were placed within its plane of symmetry, thus splitting the antenna conditionally into two arms. These arms can be considered as two independent antennas placed on different sides of the screen; each of these is characterized by the same radiation efficiency $\eta_{1r} = \eta_{2r} = \eta_r$ as the entire antenna, however their impedances and effective lengths are only half as large as the respective parameters for the entire one, specifically $Z_1 = Z_2 = Z / 2$ and $l_{1e} = l_{2e} = l_e / 2$. The vectorial radiation patterns (RPs) of the arms, $\vec{F}_1(\theta,\varphi)$ and $\vec{F}_2(\theta,\varphi)$, are two symmetrical non-intersecting parts of the entire RP, namely $\vec{F}(\theta,\varphi) = \vec{F}_1(\theta,\varphi) \cup \vec{F}_2(\theta,\varphi)$, each in the half-space of its own.

In Fig. 2, the antenna arms are represented as two two-port networks, A–1 and A–2, with a three-winding transformer in the form of a three-port network T. Assuming the transformer to be ideal, we can describe its scattering matrix as follows

$$\mathbf{S}^{\mathrm{T}} = \frac{1}{2n^2+1}\begin{pmatrix} -1 & -2n^2 & 2n \\ -2n^2 & -1 & -2n \\ 2n & -2n & -(2n^2-1) \end{pmatrix}.$$

The scattering matrix of an antenna arm, either A–1 or A–2, can be determined from Eq. (1), upon having replaced $z$ by $z/2$, which yields

$$\mathbf{S}^{\mathrm{A-1,2}} = \frac{1}{z+2}\begin{pmatrix} z+2-2r\eta_r & 2\sqrt{r\eta_r} \\ 2\sqrt{r\eta_r} & z-2 \end{pmatrix}.$$

The incident waves $a_1$ and $a_2$ at the inputs can be found from Eq. (2) upon replacing $R$ and $l_e$ in it by $R/2$ and $l_e/2$, respectively

$$a_1 = -a_2 = -j\frac{1}{4}\frac{l_e}{\sqrt{R\eta_r}}\dot{\vec{E}}^i \cdot \vec{F}(\theta,\varphi). \qquad (3)$$

By comparing Eqs. (2) and (3) it is easy to find a relationship between $a_m$, $a_1$, and $a_2$, *viz.*

$$a_1 = -a_2 = a_{in}/\sqrt{2}, \qquad (4)$$

which shows that the power $P_{in} = |a_{in}|^2$ at the antenna input is a sum of powers at its arms' inputs $P_1 + P_2 = |a_1|^2 + |a_2|^2 = |a_{in}|^2 = P_{in}$.

The two-port networks A–1 and A–2 are identical; each can be represented as a cascaded connection of the two-port network A and the transformer T1 hav-

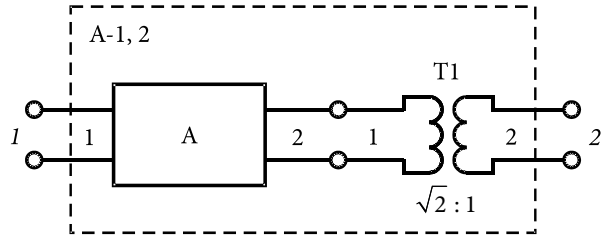


***Fig. 3.*** Representation of an antenna arm as a two-port network

ing a turns ratio of $\sqrt{2}:1$ (Fig. 3). The scattering matrix of the transformer is of the form [26]

$$\mathbf{S}^{\mathrm{T1}} = \frac{1}{3}\begin{pmatrix} 1 & 2\sqrt{2} \\ 2\sqrt{2} & -1 \end{pmatrix}.$$

This can be easily shown through the use of the equations for calculating the scattering matrix $\mathbf{S}^{(U)}$ for the cascade of two two-port networks characterized by the matrices $\mathbf{S}^{(1)}$ and $\mathbf{S}^{(2)}$ [24, 26],

$$\begin{aligned} S_{11}^{(U)} &= S_{11}^{(1)} + S_{11}^{(2)} S_{21}^{(1)} S_{12}^{(1)} / Q, \\ S_{12}^{(U)} &= S_{12}^{(1)} S_{12}^{(2)} / Q, \\ S_{21}^{(U)} &= S_{21}^{(1)} S_{21}^{(2)} / Q, \\ S_{22}^{(U)} &= S_{22}^{(2)} + S_{22}^{(1)} S_{21}^{(2)} S_{12}^{(2)} / Q, \end{aligned} \tag{5}$$

where

$$Q = 1 - S_{11}^{(2)} S_{22}^{(1)}.$$

The antenna arms A–1, 2 with their LNA–1, 2 form two channels, specifically CH–1 and CH–2 (Fig. 4), which the energy of the electromagnetic wave $\dot{\vec{E}}^{i}$ is transferred through when traveling from free space to the combiner inputs.

With the introduction of the two-port networks CH–1, 2 (Fig. 4), the block diagram of Fig. 3 is simplified to the form of Fig. 5. Denoting the scattering matrix as $\hat{\mathbf{S}}$ we can assume it known since it can be obtained through combining the two-port networks A–1, 2 and LNA–1, 2.

Now we are in a position to combine all the blocks involved in the three-port network of Fig. 5 and, by using the equations from paper [24], find its scattering matrix $\tilde{\mathbf{S}}$,

$$\tilde{\mathbf{S}} = \begin{pmatrix} \hat{S}_{11} - [1-(2n^2-1)\hat{S}_{22}]G/D & -2n^2 G/D & 2n\hat{S}_{12}/D \\ -2n^2 G/D & \hat{S}_{11} - [1-(2n^2-1)\hat{S}_{22}]G/D & -2n\hat{S}_{12}/D \\ 2n\hat{S}_{21}/D & -2n\hat{S}_{21}/D & [(2n^2+1)\hat{S}_{22} - (2n^2-1)]/D \end{pmatrix}, \tag{6}$$

where

$$D = (2n^2+1) - (2n^2-1)\hat{S}_{22} \text{ and } G = \frac{\hat{S}_{12}\hat{S}_{21}}{1+\hat{S}_{22}}.$$

## 3. Representing the SAA as a two-port network

Using its symmetry property, let us simplify the SAA block diagram shown in Fig. 5. The relationships between the incident and reflected waves at its inputs are described by the following system of equations

$$\begin{aligned} b_1 &= \tilde{S}_{11}a_1 + \tilde{S}_{12}a_2 + \tilde{S}_{13}a_3, \\ b_2 &= \tilde{S}_{21}a_1 + \tilde{S}_{22}a_2 + \tilde{S}_{23}a_3, \\ b_3 &= \tilde{S}_{31}a_1 + \tilde{S}_{32}a_2 + \tilde{S}_{33}a_3. \end{aligned} \tag{7}$$

Taking into account symmetry properties of the three-port network (Fig. 5) and the excitation condition of its inputs (Eq. (4)), we arrive at $a_2 = -a_1$ $\tilde{S}_{11} = \tilde{S}_{22}$, $\tilde{S}_{21} = \tilde{S}_{12}$, $\tilde{S}_{23} = -\tilde{S}_{13}$, and $\tilde{S}_{32} = -\tilde{S}_{31}$. Considering these relations, Eq. (7) can be transformed to the form

$$\begin{aligned} b_1 &= \tilde{S}_{11}a_1 - \tilde{S}_{21}a_1 + \tilde{S}_{13}a_3, \\ b_2 &= -\tilde{S}_{11}a_1 + \tilde{S}_{21}a_1 - \tilde{S}_{13}a_3, \\ b_3 &= \tilde{S}_{31}a_1 + \tilde{S}_{31}a_1 + \tilde{S}_{33}a_3. \end{aligned} \tag{8}$$

The relation $b_2 = -b_1$ that follows from the equation set Eq. (8) allows us to reduce this system to the form

$$\begin{aligned} b_1 &= (\tilde{S}_{11} - \tilde{S}_{21})a_1 + \tilde{S}_{13}a_3, \\ b_3 &= 2\tilde{S}_{31}a_1 + \tilde{S}_{33}a_3. \end{aligned} \tag{9}$$

Now we transform Eq. (9) by multiplying the first equation by $\sqrt{2}$ and making obvious substitutions $a_1\sqrt{2} = a_{in}$, $b_1\sqrt{2} = b_{in}$, $a_3 = a_{out}$, and $b_3 = b_{out}$.

As a result, we obtain the following system of equations to characterize the SAA as a two-port network

$$\begin{pmatrix} b_{in} \\ b_{out} \end{pmatrix} = \begin{pmatrix} \tilde{S}_{11} - \tilde{S}_{21} & \sqrt{2}\tilde{S}_{13} \\ \sqrt{2}\tilde{S}_{31} & \tilde{S}_{33} \end{pmatrix} \begin{pmatrix} a_{in} \\ a_{out} \end{pmatrix} = \mathbf{S}^{\mathrm{SAA}} \begin{pmatrix} a_{in} \\ a_{out} \end{pmatrix},$$

where $\mathbf{S}^{\mathrm{SAA}}$ is the SAA scattering matrix, which, after substitution of elements from Eq. (6), takes

the form

$$\mathbf{S}^{\mathrm{SAA}} = \begin{pmatrix} \hat{S}_{11} + (2n^2-1)\hat{S}_{12}\hat{S}_{21}/D & 2\sqrt{2}n\hat{S}_{12}/D \\ 2\sqrt{2}n\hat{S}_{21}/D & [(2n^2+1)\hat{S}_{22} - (2n^2-1)]/D \end{pmatrix}.$$

It is easy to show that the matrix $\mathbf{S}^{\mathrm{SAA}}$, coincides with the scattering matrix of the cascade of two two-port networks (Fig. 6), specifically, of the above introduced CH, and the transformer T2 with its turns ratio $\sqrt{2}n:1$.

By specifying details of the CH network shown in Fig. 6 through the use of Figs. 2 and 6, we obtain an expanded block diagram of the SAA shown in Fig. 7.

Comparing the block-diagram representations of the SAA in Figs. 1, *b* and 7, we can pick out of the latter the ABU diagram shown in Fig. 8.

## 4. Identifying ABU parameters

The ABU scattering matrix $\mathbf{S}^{\mathrm{ABU}}$ (Fig. 8) can be constructed by combining the T1, LNA, and T2 two-port networks into one by using Eq. (5). It seems better to perform this procedure numerically, since the resulting analytical expression for $\mathbf{S}^{\mathrm{ABU}}$ is quite cumbersome when $n$ is an arbitrary number. However, for some values of $n$, the calculation formulas are pretty simple, for example, for $n = 1/\sqrt{2}$ and $n = 1$, which correspond to the widely used three-winding transformers [27] and [28], respectively. When $n = 1/\sqrt{2}$, the turns ratio of T2 (see Fig. 8) is 1:1, which means absence of the transformer, and the desired formula takes the form

$$\mathbf{S}^{\mathrm{ABU}} = \begin{pmatrix} \dfrac{1+3S_{11}}{3+S_{11}} & \dfrac{2\sqrt{2}S_{12}}{3+S_{11}} \\ \dfrac{2\sqrt{2}S_{21}}{3+S_{11}} & S_{22} - \dfrac{S_{21}S_{12}}{3+S_{11}} \end{pmatrix}.$$

In the case of $n = 1$, the turns ratio of the T2 is $\sqrt{2}:1$, and the ABU scattering matrix is

$$\mathbf{S}^{\mathrm{ABU}} = \begin{pmatrix} 3 - \dfrac{8}{\mathrm{K}}(3 - S_{22}) & \dfrac{8}{\mathrm{K}}S_{12} \\ \dfrac{8}{\mathrm{K}}S_{21} & -\dfrac{1-3S_{22}}{3-S_{22}}\left(1 + \dfrac{8}{\mathrm{K}} \cdot \dfrac{S_{12}S_{21}}{1-3S_{22}}\right) \end{pmatrix},$$

where

$$\mathrm{K} = (3 + S_{11})(3 - S_{22}) + S_{12}S_{21}.$$

We will find the ABU noise matrix $\mathbf{C}^{\mathrm{ABU}}$ in the same way as its scattering matrix $\mathbf{S}^{\mathrm{ABU}}$, for which

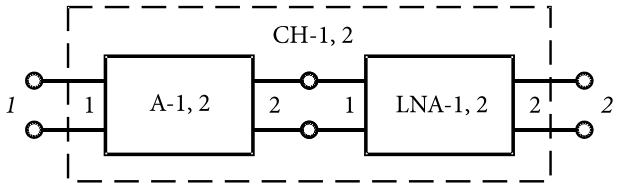


***Fig. 4.*** Block-diagram of a channel

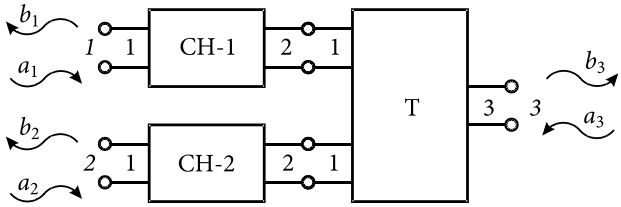


***Fig. 5.*** Simplified three-port network

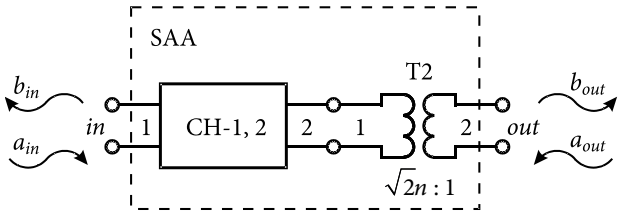


***Fig. 6.*** Reduced block-diagram of the SAA

we will need equations for calculating the matrix $\mathbf{C}^{(U)}$ of a cascade of two two-port networks characterized by the matrices $\mathbf{C}^{(1)}$ and $\mathbf{C}^{(2)}$ [24]:

$$C_{11}^{(U)} = C_{11}^{(1)} + |g|^2 C_{22}^{(1)} + 2\,\mathrm{Re}(gC_{21}^{(1)}) + |t|^2 C_{11}^{(2)},$$

$$C_{12}^{(U)} = th^* C_{11}^{(2)} + gu^* C_{22}^{(1)} + tC_{12}^{(2)} + u^* C_{12}^{(1)},$$

$$C_{21}^{(U)} = ht^* C_{11}^{(2)} + g^* uC_{22}^{(1)} + t^* C_{21}^{(2)} + uC_{21}^{(1)},$$

$$C_{22}^{(U)} = C_{22}^{(2)} + |h|^2 C_{11}^{(2)} + 2\,\mathrm{Re}(hC_{12}^{(2)}) + |u|^2 C_{22}^{(1)},$$

where

$$u = S_{21}^{(2)}/Q,\ \ t = S_{12}^{(1)}/Q,\ \ g = tS_{11}^{(2)},\ \ h = uS_{22}^{(1)}.$$

Now we present elements of the ABU **C**-matrix as derived with the use of the above equations, for two versions of the turns ratio $n$ for the transformer T (see Fig. 1, *a*):

a) $n = 1/\sqrt{2}$:

$$C_{11}^{\mathrm{ABU}} = |w|^2\, C_{11},\ \ C_{12}^{\mathrm{ABU}} = w(C_{12} + v^* C_{11}),$$

$$C_{21}^{\mathrm{ABU}} = (C_{12}^{\mathrm{ABU}})^*,$$

$$C_{22}^{\mathrm{ABU}} = C_{22} + |v|^2\, C_{11} + 2\,\mathrm{Re}(vC_{12});$$

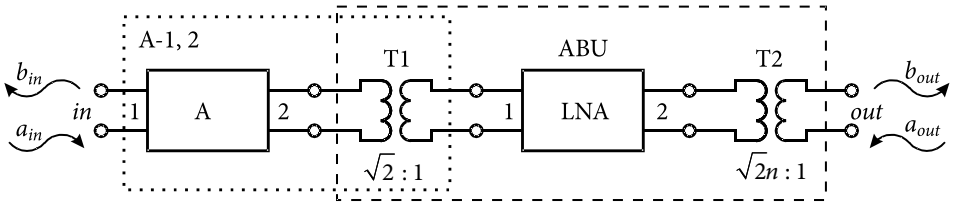


***Fig. 7.*** Expanded block-diagram of the SAA

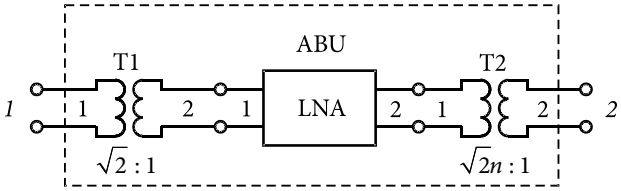


***Fig. 8.*** Block-diagram of the ABU: Final view as a two-port network

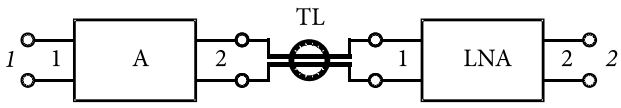


***Fig. 9.*** Block-diagram of an active antenna with a passive balun

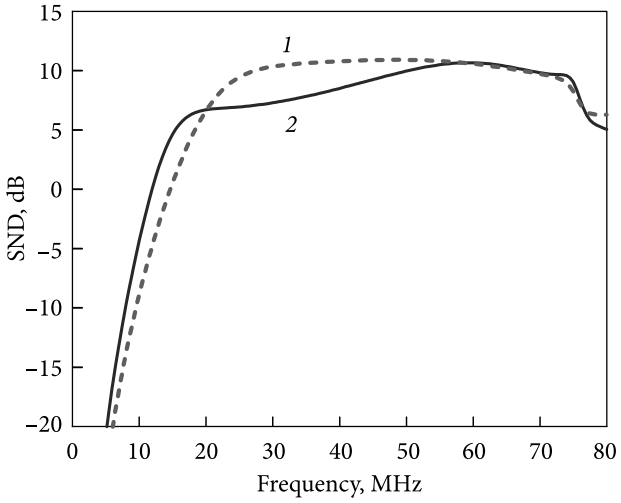


***Fig. 10.*** Frequency dependent SND of an active antenna: *1* — with a passive balun; *2* — with an ABU

b) $n=1$:

$$C_{11}^{\mathrm{ABU}} = [|w|^2 + |v|^2|q|^2 + 2\mathrm{Re}(qvw^*)]C_{11} + \\ + 2\mathrm{Re}(qw^*C_{21} + v|q|^2 C_{12}) + |q|^2 C_{22},$$

$$C_{12}^{\mathrm{ABU}} = p^*[(q|v|^2 + wv^*)C_{11} + \\ + 2q\,\mathrm{Re}(vC_{12}) + wC_{12} + qC_{22}],$$

$$C_{21}^{\mathrm{ABU}} = (C_{12}^{\mathrm{ABU}})^*,$$

$$C_{22}^{\mathrm{ABU}} = |p|^2 [|v|^2 C_{11} + 2\mathrm{Re}(vC_{12}) + C_{22}],$$

where

$$w = \frac{2\sqrt{2}}{3+S_{11}};\quad v = -\frac{S_{21}}{3+S_{11}};\quad p = \frac{2\sqrt{2}}{3-S_{22}-vS_{12}},$$

and

$$q = \frac{wS_{12}}{3-S_{22}-vS_{12}}.$$

The $\mathbf{C}^{\mathrm{ABU}}$ matrix contains complete information on noise properties of the ABU represented as a dual-port network (Fig. 8), while knowing that one can determine any of its noise parameters, such as the noise figure, minimum noise factor, optimal noise source impedance, etc. [29, 30]. At the same time, analysis of the ABU block diagram (Fig. 8) allows us commenting on the difference between its properties and those of a single LNA without resorting to any calculations. Here are some of them:

– owing to the presence of transformer T1, the ABU input impedance is twice as large as that of the LNA, $Z_{in}^{\mathrm{ABU}} = 2Z_{in}^{\mathrm{LNA}}$;

– because of presence in the ABU of transformer T2, the ABU output impedance differs from that of the LNA, being equal to $Z_{out}^{\mathrm{ABU}} = Z_{out}^{\mathrm{LNA}} / 2n^2$; in particular with $n=1$ it is $Z_{out}^{\mathrm{ABU}} = Z_{out}^{\mathrm{LNA}} / 2$, while with $n = 1/\sqrt{2}$ $Z_{out}^{\mathrm{ABU}} = Z_{out}^{\mathrm{LNA}}$;

– the minimum noise figure of the ABU is the same as that of the LNA, *i.e.* $NF_{\min}^{\mathrm{ABU}} = NF_{\min}^{\mathrm{LNA}}$ since the transformers T1 and T2 do not affect the value;

– the optimal impedance of the noise source, capable of ensuring the minimum noise figure of the ABU is twice as high as that of the source for the LNA, $Z_{opt}^{\mathrm{ABU}} = 2Z_{opt}^{\mathrm{LNA}}$.

## 5. SAA simulation

The technique developed was applied for testing the active antenna which normally makes part of the

phased array antenna of the radio telescope GURT. It employs a symmetric dipole whose design is described in detail in [31], and the ABU as a preamplifier, the circuit diagram of which can be seen in [17]. The active antenna parameters were calculated in two ways: the first approach used a three-port block diagram (Fig. 2) and required use of commercial software such as NI AWR Design Environment [32]. The other one was based on the technique developed above, being implemented within a simple computer mathematics of MathCad type. Both methods showed identical calculated results for all electrical and noise parameters of the active antenna under study, which was fully confirmed by the experimental results of paper [31].

Also, it would be of interest to compare the parameters of two symmetrical active antennas, namely one containing an ABU and the other involving an LNA and a transmission-line (TL) transformer [1] in the capacity of a passive balun. Both antennas make use of passive antennas and LNAs of the same design, and block diagrams of the antennas under comparison are shown in Figs. 7 and 9, respectively. The electrical length of the TL transformer is assumed to be negligibly small compared with the free-space wavelength. The electrical and noise parameters of the two antennas were calculated within the technique that had been given a detailed description in papers [31] and [33]. One such parameter that can significantly affect an active antenna's sensitivity toward fluctuations (as well as such of a radio telescope) is the SND (Sky Noise Dominance). It is determined as the ratio $\mathrm{SND} = T_{ext}/T_{int}$, where $T_{int}$ stands for the external noise temperature of the active antenna receiving the Galactic and/or extragalactic radiation, while $T_{int}$ is its intrinsic noise temperature. The higher the SND, the smaller is the amount of reduction in antenna sensitivity due to internal noise. The lower SND limit is 6 dB, which corresponds to an acceptable level of sensitivity reduction, which is easily compensated for by a slight increase in the signal integration time [9].

Fig. 10 shows frequency dependences of the SNDs belonging to the active antennas being compared. Their differences are pretty clearly visible, as they are caused by different levels of impedance mismatch between the dipoles with the LNA or the ABU. At frequencies below 15 MHz, the SND of the GURT antenna with an ABU is noticeably higher than that of the antenna with a passive balun. This is explained by the presence of a matching circuit at the ABU input, specially included for expanding the operating frequency band of the radio telescope towards lower frequencies. Note, however, a certain decrease in the SND, seen in the middle part of the 15—55 MHz range, where its level is lower than that of the antenna with a passive balun. At frequencies above 55 MHz, the SNDs of the antennas under comparison are practically equal.

So, when both of the antennas under comparison are capable of providing the same level of impedance matching, they have the same SNDs; however, when creating ground-based LF radio telescopes, preference is still given to antennas with ABUs, as they are more resistant to intermodulation interference. The only exceptions to this rule may be the radio telescopes operating in an environment without substantial interference, for example, on the far side of the Moon [34].

## Conclusions

An active receiving antenna, which consists of a passive symmetrical antenna and an ABU has been considered. The ABU comprises a differential pair of identical LNAs and a three-winding differential-input single-ended transformer. The conventional representation of an ABU in the form of a three-port network has been converted, through equivalent transformations, into such for a two-port network. That has allowed constructing the active antenna's block diagram, showing it as a cascaded connection of two two-port networks, of which the first one is associated with a passive antenna and the second with an ABU.

Analytical relations have been derived that permit calculating the scattering matrix and the correlation matrix of noise waves within the two-port network associated with the active antenna, proceeding from the assumption that parameters of the passive antenna and of the LNA are known. These matrices should ultimately allow us to determine all operating parameters of the active receiving antenna. The relationships obtained permit a greatly simplified analysis of a symmetrical active antenna with an ABU without resorting to any special software for solving the problem.

A numerical example is presented where two symmetrical active antennas are compared, specifically one using an ABU and the other a single amplifier with a passive balun, with the intent of applying them as elements of a phased array antenna for a low-frequency radio telescope. The calculations show that none of the antennas demonstrate a noticeable advantage over the other — in what concerns its SND and, hence, the fluctuation sensitivity. Thus, preference should be given to antennas with an ABU, as they are more resistant to intermodulation interference, which is very important for correctly operating any ground-based LF radio telescope.

***Acknowledgment.*** *This work was supported by the National Academy of Sciences of Ukraine, Research Project No. 4.1/25П.*

REFERENCES

1. Sevick, J., 2001. *Transmission Line Transformers*. 4th ed. Atlanta, GA, USA: Noble Publishing.
2. Konovalenko, A., Sodin, L., Zakharenko, V., Zarka, P., Ulyanov, O., Sidorchuk, M., Stepkin, S., Tokarsky, P., Melnik, V., Kalinichenko, N., Stanislavsky, A., Koliadin, V., Shepelev, V., Dorovskyy, V., Ryabov, V., Koval, A., Bubnov, I., Yerin, S., Gridin, A., Kulishenko, V., Reznichenko, A., Bortsov, V., Lisachenko, V., Reznik, A., Kvasov, G., Mukha, D., Litvinenko, G., Khristenko, A., Shevchenko, V. V., Shevchenko, V. A., Belov, A., Rudavin, E., Vasylieva, I., Miroshnichenko, A., Vasilenko, N., Olyak, M., Mylostna, K., Skoryk, A., Shevtsova, A., Plakhov, M., Kravtsov, I., Volvach, Y., Lytvinenko, O., Shevchuk, N., Zhouk, I., Bovkun, V., Antonov, A., Vavriv, D., Vinogradov, V., Kozhin, R., Kravtsov, A., Bulakh, E., Kuzin, A., Vasilyev, A., Brazhenko, A., Vashchishin, R., Pylaev, O., Koshovyy, V., Lozinsky, A., Ivantyshin, O., Rucker, H. O., Panchenko, M., Fischer, G., Lecacheux, A., Denis, L., Coffre, A., Grießmeier, J.-M., Tagger, M., Girard, J., Charrier, D., Briand, C., and Mann, G., 2016. The modern radio astronomy network in Ukraine: UTR-2, URAN and GURT. *Exp. Astron.*, **42**(1), pp. 11—48. DOI: 10.1007/s10686-016-9498-x
3. Gonzalez-Esparza, A., Carrillo, A., Andrade, E., Jeyakumar, S., Perez-Enriquez, R., and Kurtz, S., 2002. The MEXART interplanetary scintillation array in Mexico. *Geofis. Int.*, **43**(1), pp. 61—73. DOI: 10.22201/igeof.00167169p.2004.43.1.215
4. Oraizi, H., 2016. Impedance Matching and BALUNs. In: Z.N. Chen, ed. *Handbook of Antenna Technologies*. Singapore: Springer Nature, pp. 3350—3428.
5. Costain, C., Lacey, J., and Roger, R., 1969. Large 22-MHz array for radio astronomy. *IEEE Trans. Antennas Propag.*, **17**(2), pp. 162—169. DOI:10.1109/TAP.1969.1139409
6. Sastry, Ch.V., 1995. The decameter and meter wave radiotelescopes in India and Mauritius. *Space Sci. Rev.*, **72**, pp. 629—654. DOI: 10.1007/BF00749008
7. Abidi, A.A., 2003. General Relations between IP2, IP3, and Offsets in Differential Circuits and the Effects of Feedback, *IEEE Trans. Microw. Theory Techn.*, **51**(5), pp. 1610—1612. DOI: 10.1109/TMTT.2003.810147
8. Falkovich, I.S., Konovalenko, A.A., Gridin, A.A., Sodin, L.G., Bubnov, I.N., Kalinichenko, N.N., Rashkovskii, S.L., Mukha, D.V., and Tokarsky, P.L., 2011. Wide-band high linearity active dipole for low frequency radio astronomy. *Exp. Astron.*, **32**(2), pp. 127—145. DOI: 10.1007/s10686-011-9256-z
9. Ellingson, S.W., Taylor, G.B., Craig, J., Hartman, J., Dowell, J., Wolfe, C.N., Clarke, T.E., Hicks, B.C., Kassim, N.E., Ray, P.S., Rickard, L.J., Schinzel, F.K., and Weiler, K.W., 2013. The LWA1 Radio Telescope, *IEEE Trans. Antennas Propag.*, **61**(5), pp. 2540—2549. DOI: 10.1109/TAP.2013.2242826
10. Stewart, K.P., Hicks, B.C., Ray, P.S., Crane, P.C., Kassim, N.E., Bradley, R.F., and Erickson, W.C., 2004. LOFAR antenna development and initial observations of solar bursts. *Planet. Space Sci.*, **52**(15), pp. 1351—1355. DOI: 10.1016/j.pss.2004.09.014
11. Ellingson, S.W., Simonetti, J.H., and Patterson, C.D., 2007. Design and Evaluation of an Active Antenna for a 29—47 MHz Radio Telescope Array. *IEEE Trans. Antennas Propag.*, **55**(3), pp. 826—831. DOI: 10.1109/TAP.2007.891866
12. Rosa, G.S., Schuch, N.J., Gomes, N.R., Bergmann, J.R., Echer, E., and Machado, R., 2012. Inexpensive Interferometer for Low Frequency Radio Astronomy. *Journal of Communication and Information Systems (JCIS)*, **27**(1). DOI: 10.14209/jcis.2012.5
13. De Lera Acedo E., Razavi-Ghods, N., Troop, N., Drought, N., and Faulkner, A.J., 2015. SKALA, a log-periodic array antenna for the SKA-low instrument: design, simulations, tests and system considerations. *Exp. Astron.*, **39**, pp. 567—594. DOI: 10.1007/s10686-015-9439-0
14. Shaw, R.D., Hay, S.G., and Ranga, Y., 2012. Development of a Low-Noise Active Balun for a Dual-Polarized Planar Connected Array Antenna for ASKAP. In: *2012 Int. Conf. Electromagnetics in Advanced Applications*. Cape Town, South Africa, 02—07 Sept. 2012. DOI: 10.1109/ICEAA.2012.6328666
15. Sutinjo, A.T., Colegate, T.M., Wayth, R.B., Hall, P.J., de Lera Acedo, E., Booler, T., Faulkner, A.J., Feng, L., Hurley-Walker, N., Juswardy, B., Padhi, S.K., Razavi-Ghods, N., Sokolowski, M., Tingay, S.J., and Bij de Vaate, J.G., 2015. Characterization of a Low-Frequency Radio Astronomy Prototype Array in Western Australia. *IEEE Trans. Antennas Propag.*, **63**(12), pp. 5433—5442. DOI: 10.1109/TAP.2015.2487504

16. Zarka, P., Denis, L., Tagger, M., Girard, J., Coffre, A., Dumez-Viou, C., Taffoureau, C., Charrier, D., Bondonneau, L., Briand, C., Casoli, F., Cecconi, B., Cognard, I., Corbel, S., Dallier, R., Ferrari, C., Grießmeier, J-M., Loh, A., Martin, L., Pommier, M., Semelin, B., Tasse, C., Theureau, G., Tremou, E., Hellbourg, G., Konovalenko, A., Koopmans, L., Tokarsky, P., Ulyanov, O., Vermeulen, R., and Zakharenko, V., 2020. The low-frequency radio telescope NenuFAR. In: *Proc. XXXIII$^{rd}$ URSI General Assembly and Scientific Symposium*. Rome, Italy, 29 August — 5 Sept. 2020, J01-02. [viewed 20.08.2024]. Available from: https://www.ursi.org/proceedings/procGA20/papers/URSIGASS2020SummaryPaperNenuFARnew.pdf
17. Tokarsky, P.L., Konovalenko, A.A., Yerin, S.N., and Bubnov, I.N. An Active Antenna Subarray for the Low-Frequency Radio Telescope GURT–Part I: Design and Theoretical Model. *IEEE Trans. Antennas Propag.*, **67**(12), pp. 7304—7311. DOI: 10.1109/TAP.2019.2927841
18. Bubnov, I.N., Konovalenko, O.O., Tokarsky, P.L., Korolev, O.M., Yerin, L.O., and Stanislavsky, S.M. 2021. Creation and approbation of a low-frequency radio astronomy antenna for studying objects of the Universe from the farside of the Moon. *Radio Phys. Radio Astron.*, **26**(3), pp. 197—210. DOI: https://doi.org/10.15407/
19. Stewart, K., Hicks, B., Paravastu, N., Bradley, R., Parashare, C., Erickson, W., Gross, C., Polisensky, E., Crane, P., Ray, P., Kassim, N., and Weiler K., 2005. Recent Progress in Active Antenna Designs for the Long Wavelength Array (LWA), 2005. In: *Proc. URSI General Assembly*. New Delhi, India, 23—29 Oct. 2005. [viewed 20.08.2024]. Available from: https://www.ursi.org/proceedings/procGA05/pdf/J03-P.15(0981).pdf
20. Bradley, R.F., and Parashare, C.R., 2005. Evaluation of the NRL LWA Active Balun Prototype. *NRAO NTC-DSL Laboratory Report 01*, *Rev. A* [viewed 20.08.2024]. Available from: https://www.gb.nrao.edu/electronics/edtn/edtn220.pdf
21. Korolev, A.M., Zakharenko, V.V., and Ulyanov, O.M., 2016. Radio astronomy ultra-low-noise amplifier for operation at 91 cm wavelength in high RFI environment. *Exp. Astron.*, **41**(1—2), pp. 215—221. DOI: https://doi.org/10.1007/s10686-015-9466-x
22. Sutinjo, A.T., Ung, D.C.X., and Juswardy, B., 2018. Cold-Source Noise Measurement of a Differential Input Single-Ended Output Low-Noise Amplifier Connected to a Low-Frequency Radio Astronomy Antenna. *IEEE Trans. Antennas Propag.*, **66**(10), pp. 5511—5520. DOI: 10.1109/TAP.2018.2854285
23. Prinsloo, D.S., Maaskant, R., Ivashina, M.V., and Meyer, P., 2014. Mixed-Mode Sensitivity Analysis of a Combined Differential and Common Mode Active Receiving Antenna Providing Near-Hemispherical Field-of-View Coverage. *IEEE Trans. Antennas Propag.*, **32**(2), pp. 3951—3961. DOI: 10.1109/TAP.2014.2322896
24. Dobrowolski, J.A., 2016. *Scattering Parameters in RF and Microwave Circuits Analysis and Design*. Norwood, MA, USA: Artech House.
25. Tokarsky, P.L., 2020. Antenna Analytical Representation by a Two-Port Network. *Int. J. Antennas Propag.*, 2020, id. 2609747. DOI: 10.1155/2020/26097473
26. Gupta, K., Garg R., and Chandra, R., 1981. *Computer-aided design of microwave circuits*. Dedham, MA, USA: Artech House.
27. Flux Coupled Balun 1:2. [viewed 20.08.2024]. Available from: https://www.macom.com/products/product-detail/MABA-011050
28. RF Flux Coupled Transformer 1:4, E-Series. [viewed 20.08.2024]. Available from: https://www.macom.com/products/product-detail/MABAES0031
29. Russer, P., and Muller, S., 1990. Noise analysis of linear microwave circuits. *Int. J. Numer. Model. El.*, **3**, pp. 287—316. DOI: 10.1002/jnm.1660030408
30. Pospieszalski, M.W., 2010. Interpreting Transistor Noise. *IEEE Microwave Mag.*, **11**(6), pp. 61—69. DOI: 10.1109/MMM.2010.937733
31. Tokarsky, P.L., Konovalenko, A.A., and Yerin S.N., 2017. Sensitivity of an Active Antenna Array Element for the Low-Frequency Radio Telescope GURT. *IEEE Trans. Antennas Propag.*, **65**(9), pp. 4636—4644. DOI: 10.1109/TAP.2017.2730238
32. Tokarsky, P.L., Konovalenko, A.A., Yerin, S.N., and Bubnov I.N., 2016. Sensitivity of Active Phased Antenna Array Element of GURT Radio Telescope. *Radio Phys. Radio Astron.*, **21**(1), pp. 48—57. DOI: 10.15407/rpra21.01.048
33. Hicks, B.C., Paravastu-Dalal, N., Stewart, K.P., Erickson, W.C., Ray, P.S., Kassim, N.E., Burns, S., Clarke, T., Schmitt, H., Craig, J., Hartman, J., and Weiler, K.W., 2012. A wide-band, active antenna system for long wavelength radio astronomy. *Publ. Astron. Soc. Pac.*, **124**(920), pp. 1090—1104. DOI: 10.1086/668121
34. Tokarsky, P.L., Konovalenko, A.A., and Modelski, J.W., 2023. An Active Ribbon Dipole as an Array Element Prototype for the Lunar Very Low Frequency Radio Telescope. *IEEE Access*, **11**, pp. 75225—75235. DOI: 10.1109/ACCESS.2023.3294694

*Received 02.09.2024*

*П.Л. Токарський*

Радіоастрономічний інститут НАН України
вул. Мистецтв, 4, м. Харків, 61002, Україна

# ЕЛЕКТРИЧНІ ТА ШУМОВІ ВЛАСТИВОСТІ СИМЕТРИЧНОЇ АНТЕНИ З АКТИВНИМ СИМЕТРУВАЛЬНИМ ПРИСТРОЄМ

**Предмет і мета роботи.** У статті розглядається активна приймальна антена, що складається з симетричної пасивної антени та активного симетрувального пристрою у вигляді диференціальної пари ідентичних малошумівних підсилювачів і триобмоткового диференціального вхідного однотактного трансформатора. Метою роботи є розробка моделі такої активної антени, поданої як еквівалентний чотириполюсник з аналітично визначеними електричними та шумовими параметрами.

**Методи та методологія.** Дослідження базується на методах теорії антен і теорії шумних багатополюсників. Пасивна антена є умовно розділеною на два однакових плеча, кожне з яких розглядається як окрема незалежна антена, що дозволяє подати всю активну антену як шестиполюсник. Потім, враховуючи антисиметричне збудження цього шестиполюсника, його було перетворено на каскадне з'єднання двох чотириполюсників. Перший відповідає пасивній антені, а другий — активному симетрувальному пристрою, що складається з одного малошумівного підсилювача з доданими трансформаторами на вході і виході.

**Результати.** З використанням блок-схеми активної антени, яка розглядається як чотириполюсник, було отримано аналітичні вирази для розрахунку її матриці розсіяння та кореляційної матриці шумових хвиль. Це дозволяє оцінити електричні та шумові параметри симетричної антени з активним симетрувальним пристроєм. Наведено числовий приклад, який дозволяє порівняти параметри двох симетричних активних антен, в одному з котрих використовується активний балун, а в іншому — малошумівний підсилювач із пасивним симетрувальним пристроєм.

**Висновки.** Розроблено блок-схеми пристроїв і отримано розрахункові співвідношення, що дозволяють значно спростити аналіз антен з активними симетрувальними пристроями без залучення будь-якого спеціалізованого програмного забезпечення. Результати можуть виявитися корисними для розрахунку параметрів низькочастотних радіотелескопів, які використовують подібні антени як елементи фазованих антенних решіток.

***Ключові слова:*** *симетрична антена, активний симетрувальний пристрій, чотириполюсник, матриця розсіяння, кореляційна матриця шумових хвиль.*